mater.scichina.com link.springer.com

Sci China Mater 2025, 68(8): 2860–2867 https://doi.org/10.1007/s40843-025-3445-x



HF-free synthesis of high-entropy MXene-PVA composite film and its flexible nanogenerator

Fumei Yang, Kam Lin Chan, Zehan Wu, Fangqing Zhao, Man Chung Wong, Sin-Yi Pang and Jianhua Hao*

ABSTRACT MXene exhibits notable piezoelectric properties, making it a promising material for high-performance piezoelectric nanogenerators (PENGs) in next-generation smart wearable devices and bioelectronics. However, current MXene-based PENGs face challenges such as insufficient mechanical robustness, low piezoelectric response, and limited long-term functionality. These limitations primarily stem from the small effective area and low strain levels of MXene nanosheets. Here, we constructed a high-entropy TiVCr-MoC₃T_r MXene composite film by leveraging strong hydrogen bonding interactions between MXene and polyvinyl alcohol (PVA), which was further developed into a self-powered flexible nanogenerator. The resulting device exhibited a significant piezoresponse with output signals of 500 mV and 790 pA under a compressive force of 3.47 N, along with considerable long-term functionality over 1500 cycles. Moreover, a hydrofluoric-free etching approach was employed to synthesize the high-entropy MXene nanosheets, which ensures the safety and biocompatibility for bioelectronics applications. This work highlights the potential of high-entropy MXene for sustainable applications in wearable electronics and energy harvesting.

Keywords: $TiVCrMoC_3T_x$, high-entropy MXene, hydrofluoric-free etching, MXene-PVA composite film, flexible nanogenerator

INTRODUCTION

MXene, a class of two-dimensional materials, has emerged as a versatile material with a plethora of exceptional characteristics, including vast surface area, excellent catalytic performance, impressive mechanical properties, high tunability, and notable piezoelectric sensitivity [1–5]. These attributes have propelled MXene into the spotlight across diverse applications, such as catalysis, sensing technologies, and energy devices [6–8]. Notably, MXene exhibits strong piezoelectric properties due to the non-centrosymmetric lattice from the multi-atomic lattice structure and tunable functional groups, enabling to practical applications in flexible nanogenerators [5,9–12].

Recently, high-entropy MXenes incorporating multiple transition metallic elements have garnered attention for their superior physiochemical properties compared to their conventional counterparts [13–15]. The asymmetric interlayer segregation of atoms in high-entropy MXenes underscores their unique electrical behavior, which is crucial for their piezoelectric

characteristics [15]. While conventional hydrofluoric acid (HF) etching remains a common method for layered MXene synthesis due to its efficient delamination and high yields, concerns persist regarding safety and environmental impact owing to its corrosiveness and toxicity. Alternatively, HF-free etching routes, such as alkali etching, molten salt etching, and electrochemically etching, offer safer approaches for MXene production [8,16,17]. Despite these advancements, achieving piezotronic applications for MXene nanosheets remains challenging due to size limitations and low strain levels. To address this, MXene nanosheets can be engineered into self-supporting thin films through facile methods like vacuum filtration, which could consolidate the exceptional properties of individual MXene nanosheets and enable to their development in large-scale and array-based applications [18]. However, their inherent random stacking would undermine stability and strain tolerance under external conditions like mechanical stress, thereby hindering their practical applicability [19]. The MXene films, capable of preserving structural integrity and performance stability, are highly desirable. One effective strategy involves the integration of polymers into MXene matrices through robust interactions, leveraging dynamic covalent or non-covalent bonds to tailor the physical and chemical properties of layered materials and developing adaptable composite thin films suitable for flexible sensing applications. Polyvinyl alcohol (PVA) serves as the matrix material in piezoelectric composite structures, providing a flexible base for embedding functional nanomaterials. Furthermore, by enhancing the mechanical properties of the composite films, PVA strengthens them against mechanical stress and deformation, thereby playing a crucial role for preserving the structural integrity of the nanogenerators during device operation [20].

Based on this strategy, this work proposes the utilization of PVA as a polymer linker to establish strong interactions through hydrogen bonding with high-entropy MXene nanosheets. This approach effectively engineers a composite film characterized by high chemical stability and good biocompatibility [20]. Here, the high-entropy MXene TiVCrMoC $_3$ T $_x$ nanosheets were synthesized by a thermal-assisted electrochemical HF-free etching approach, which is safe and facile to achieve environmentally friendly synthesis [8]. Moreover, TiVCrMoC $_3$ T $_x$ nanosheets with a non-centrosymmetric structure could contribute to a robust piezoelectric response [14,15]. Meanwhile, the MXene-PVA composite films exhibited favorable mechanical properties, making them promising for applications in smart and wearable electronics. Therefore, by bridging the gap for stable and flexible piezoelectric nanomaterials adaptable to mechanical deforma-

Department of Applied Physics, The Hong Kong Polytechnic University, Hong Kong 999077, China

^{*} Corresponding author (email: jh.hao@polyu.edu.hk)

SCIENCE CHINA Materials

ARTICLES

tion, MXene-PVA composite films were further developed into piezoelectric nanogenerators (MXene/PVA-PENGs). Notably, the MXene/PVA-PENG device exhibited significant piezoresponse signals (500 mV and 790 pA) at 3.47 N compressive force, surpassing previously reported MXene nanosheet-based devices [5,9]. Furthermore, this flexible nanogenerator demonstrated long-term functionality over 1500 cycles, showcasing high stability and capability. These results highlight the immense potential of high-entropy MXene nanosheets for applications in energy harvesting and healthcare electronic systems.

EXPERIMENTAL SECTION

Synthesis of TiVCrMoC₃T_r nanosheets

The high-entropy MXene TiVCrMoC₃T_r nanosheets were synthesized using a thermal-assisted electrochemical HF-free etching approach. Prior to the synthesis process, carbon fiber cloths (W0S1002, CeTech) were deeply cleaned in acetone and ethanol through sonication to eliminate any organic contaminants on the surface. Subsequently, the clothes underwent surface modification with HNO₃ (63 wt.% %, Sigma) for 6 h at 125 °C under reflux conditions, followed by neutralization with a 1 M NaOH solution. Then the clothes were rinsed thrice with deionized water and dried at 60 °C in an oven. The MAX precursor (TiVCrMoAlC₃, >99%, Laizhou Kai Ceramic Material Co., Ltd.) was initially blended with carbon black in a 95:5 ratio, dispersed in 1% PVA as an adhesion agent to create a composite electrode, and uniformly applied onto the carbon fiber cloths. The etching process was carried out at an etching voltage of 1 V and a temperature of 55 °C in a dilute HCl electrolyte to enhance etching efficiency and yield. The process could be described as follows:

Since the MXene sheets are stacked together by van der Waals forces, delamination is essential to increase the yield of TiVCr-MOC₃T_x nanosheets. This involves intercalating the sheets with tetrabutylammonium hydroxide (TBAOH) solvent, followed by sonication. After adding TBAOH to the TiVCrMoC₃T_x suspension, the mixture is stirred at room temperature for 24 h and then subjected to bath sonication for 3 h. Following sonication, the treated TiVCrMoC₃T_x MXene is centrifuged at 3500 r/min for 15 min to collect the suspension of nanosheets.

Preparation of MXene-PVA composite film

After the synthesis of high-entropy MXene nanosheets, the MXene-PVA composite film was also prepared as follows. The initial step involved mixing the as-prepared 5 mg/mL high-entropy MXene solution thoroughly with a 10% PVA aqueous solution in a 1:1 ratio, ensuring complete homogenization. This mixture was then carefully poured into a mold and left to dry overnight, resulting in the formation of a uniform composite film. After drying, the composite film was peeled off and subsequently integrated into a piezoelectric nanogenerator device connected to conductive Ni electrodes. The thickness of the composite film was measured to be approximately 400 µm.

Characterizations and device measurements

As for material characterization, the X-ray diffraction (XRD) patterns of the high-entropy MXene were acquired using the Rigaku SmartLab 9kW-Advance instrument. For morphological

analysis, the high-entropy MXene nanosheets were examined through scanning electron microscopy (SEM, Zeiss Merlin), transmission electron microscopy (TEM, JEOL JEM-2100F) and atomic force microscopy (AFM, Asylum MFP-3D Infinity), respectively. Raman spectroscopy was conducted with a micro-Raman spectrometer (Witec alpha300 R) equipped with a Zeiss EC Epiplan 50x objective lens, employing an excitation wavelength of 532 nm and a laser power of 2 mW to investigate the structural characteristics of the material. The mechanical property of the MXene-PVA composite film was investigated via a dynamic mechanical analyzer (Tensile mode, Mettler Toledo DMA1). The electric polarization-electric field (P-E) loops were measured via Premier II Ferroelectric Tester. The dielectric properties were recorded by an impedance analyzer (Keysight/ Agilent 4294A Precision Impedance Analyzer). Before the electrical measurements, the samples were coated with 50 nm gold electrodes via e-beam evaporation. To evaluate device performance, an oscillator (LeCroy WaveSurfer 62Xs) and a low-noise current preamplifier (Stanford Research Systems Model SR570) were utilized. The output performance measurements were carried out under periodic compressive strains applied by a linear motor.

RESULTS AND DISCUSSION

The atomic structure of TiVCrMoC₃T_x MXene nanosheets is demonstrated in Fig. 1a. Four layers of transition metal atoms sandwiched between carbon layers, while the outer metal layers are bonded to functional groups (Tx, such as -O, -OH and -Cl) [13]. These outermost metal atoms form active bonds with functional groups, whose asymmetric distribution breaks the inversion symmetry of the crystal structure [5,13]. Here, the layered TiVCrMoC₃T_x MXene nanosheets were synthesized by the thermal-assisted electrochemical HF-free etching approach, and the delamination of layered MXene nanosheets by etching the Al layers from the MAX precursor is first investigated. According to the XRD patterns (supplementary material, Fig. S1a), the peaks of $TiVCrMoC_3T_x$ match well with the previouslyreported results [13]. The (00l) peaks of TiVCrMoC₃T_x shift to the left, while no obvious Al-Mo peaks appear in TiVCrMoC₃T_x, indicating the effective delamination from the MAX phase. In the Raman spectra (supplementary material, Fig. S1b), the increase and red shift of characteristic peaks (near 200 and 700 cm⁻¹) of the resulting TiVCrMoC₃T_x nanosheets confirms the removal of Al layers from their parent MAX phase [21-26]. Besides, the broad peaks located in the range of 1200-1700 cm⁻¹ are attributed to the D and G bands of carbon [27,28]. These results confirm the effective removal of Al layers from the MAX phase and the successful formation of MXene nanosheets. It is important to note that our synthetic approach intentionally produces multilayered MXene structures rather than focusing on monolayer exfoliation, as multilayered MXene is more suitable for our target application, as it is mixed with polymer. TEM and AFM results (Supplementary material, Figs S2 and S3) confirm the successful preparation of these multilayered structures with thicknesses appropriate for the electromechanical applications described in this work. Besides, a comparative table summarizes key parameters of various HF-free MXene synthesis approaches, as shown in Table S1. Operating at mild temperatures (25–80 °C) with diluted HCl in ambient air, our approach offers significant advantages in safety and simplicity compared to hightemperature methods requiring inert atmospheres. With rea-

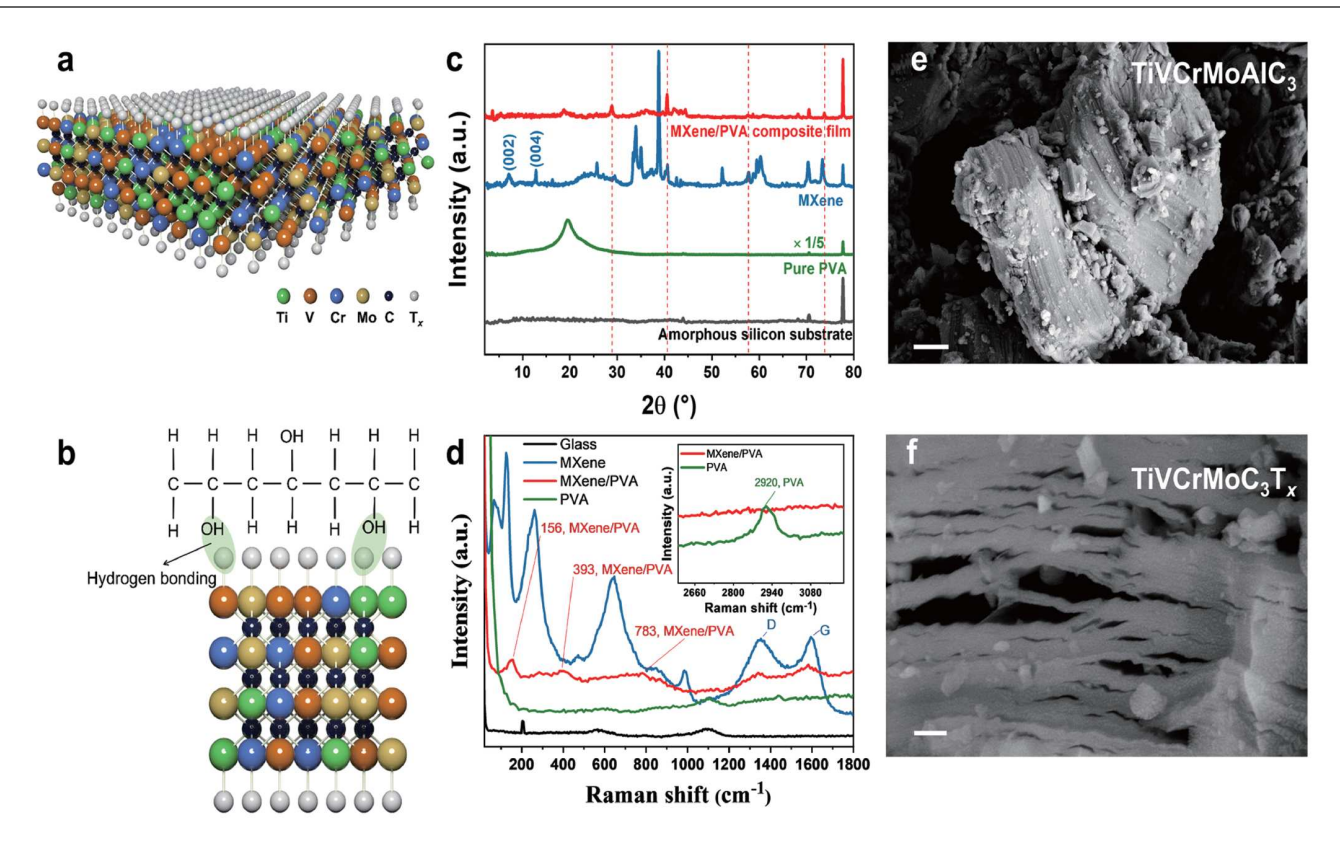


Figure 1 Structure and characterization of TiVCrMoAlC₃ MAX precursor, the resulting TiVCrMoC₃T_x layered MXene nanosheets and MXene-PVA composite film. (a) Atomic structure of a single TiVCrMoC₃T_x nanosheet. (b) The schematic illustration of the MXene-PVA composite film with cross-linked structures. (c) XRD patterns. (d) Raman spectra. (e, f) SEM images of TiVCrMoAlC₃ MAX (scale bar: 2 μ m) and TiVCrMoC₃T_x MXene (scale bar: 200 nm).

sonable yield and simple equipment requirements, this synthesis method strikes a good balance between accessibility, safety, and environmental sustainability while expanding the range of achievable MXene compositions. In addition, the fluorine-free MXenes exhibit markedly improved biocompatibility, showing negligible cytotoxicity compared to fluorinated MXenes showing significant cytotoxic effects due to fluoride ion release during oxidative degradation [29,30].

In order to achieve large-scale MXene thin films with high stability and good mechanical properties for practical applications, the PVA with flexibility, natural compatibility, and degradability is used as the matrix material in composite structures, providing a flexible and durable matrix for embedding functional materials [31]. Besides, PVA can also improve the mechanical properties of the composite, making it more robust to mechanical stress and deformation, which is important for maintaining the structural integrity of the nanogenerators during operation. The -OH on PVA chains could guide MXene nanosheets to self-assemble stacking with strong hydrogen bonding [20,31]. As shown in Fig. 1b, the PVA was employed as a cross-linker to form a network with high-entropy MXene, showing the intermolecular interaction in the strong hydrogen bonding. The mechanical properties were measured by a dynamic mechanical analyzer, as shown in Supplementary material, Fig. S2. From the stress-strain curve (Supplementary material, Fig. S4), it could be obtained that the Young's modulus of 40 µm-thick MXene-PVA thin film is 2 GPa, while the Young's modulus of pure PVA film is 1 GPa. This mechanical strength improvement is attributed to strong hydrogen bonding between MXene sheets and PVA chains, suggesting that good mechanical strength of the MXene-PVA composite film for practical applications.

After confirmation of the delamination of layered MXene nanosheets and the interaction of MXene and PVA, we further investigate the characterization of the high-entropy MXene-PVA composite film. Compared to the XRD pattern of pristine highentropy MXene, the (002) peak of MXene-PVA composite film shifts toward lower angles, suggesting the increase of d-spacing [32], as shown in Fig. 1c. This change is attributed to the strong interaction between MXene and PVA, with the formation of hydrogen bonding. From Fig. 1d, three major Raman peaks correspond to Ti-C vibrations [33,34]. Besides, compared to the pristine materials, the Raman response of the MXene-PVA composite film decreases and is blue-shifted due to the strong interaction of PVA chains. Furthermore, the SEM images offered detailed insights into the morphology of MXene nanosheets (Fig. 1f), showing uniform and layered nanosheets with accordion-like texture after etching from the bulk MAX precursor, showing smooth surfaces without any delamination (Fig. 1e). These characterizations emphasize the good quality of the layered MXene nanosheets and the MXene-PVA composite film, promising for a wide range of advanced technological applications. Moreover, the P-E loop and dielectric properties were also performed to evaluate the electrical properties, as shown in Supplementary material, Figs S5 and S6. The transition from lossy capacitor behavior (pure PVA) to resistor-like behavior (MXene-PVA composite) in P-E loop measurements suggests increased conductivity and interfacial polarization in MXene-PVA composite film, which can facilitate piezoelectric charge generation. The introduction of MXene into the PVA matrix

SCIENCE CHINA Materials

ARTICLES

slightly increases the dielectric constant, indicating enhanced polarization capability, which is favorable for piezoelectric performance. With increasing frequency, the dielectric loss of the MXene-PVA composite film initially decreased and subsequently increased. This reduction in dielectric loss at low frequencies can be attributed to the rapid decrease in interfacial leakage current, which results from the attenuation of interfacial polarization between PVA and MXene. And the slight increase in dielectric loss at higher frequencies results from the hysteresis associated with dipole orientation within the polymer matrix [33,35]. Besides, the low leakage current at pico-ampere level prevents the loss of generated polarization charges and ensures that the output signals are both detectable and reliable. Moreover, the MXene-PVA composite film also demonstrates the enhanced biocompatibility and scalability, endowing the functionality for practical applications [29,30].

The MXene-PVA composite film was further developed into a flexible piezoelectric nanogenerator. The experimental setup for output performance testing is illustrated in Fig. 2a. The MXene-PVA composite film was first connected to Ni electrodes (the inset of Fig. 2a), and then attached to the sample stage. A period compressive force driven by a linear motor would be applied to the MXene/PVA-PENG device. To exclude the influence of the triboelectric effect on the observed piezoelectric behavior of the MXene-PVA composite, a series of carefully controlled experiments were conducted. The electrodes were kept in firm contact with the film to minimize surface friction, and the mechanical deformation was applied via uniaxial compression, thus avoiding relative sliding between the film and electrodes. The output performance testing was performed without conventional poling procedures due to the piezoelectric behavior of TiVCrMoC₃T_x. and the interfacial interactions between MXene and polymer [5,9,36].

The high-entropy configuration in TiVCrMoC₃T_x MXene introduces a diverse distribution of metal elements, leading to

lattice distortions and symmetry breaking. In high-entropy materials, the multi-atomic distortions (i) stabilize single-phase structures, (ii) amplify local symmetry breaking and polar displacement, (iii) soften elastic moduli to boost electromechanical coupling, and (iv) enrich domain structures and facilitate polarization rotation [37]. Similar behavior has been observed in other high-entropy materials (such as high-entropy perovskites and $Mo_{1-x}W_xS_2$) [38,39], where compositional complexity contributes to enhanced functional properties. To analyze the piezoelectric behavior of high-entropy TiVCrMoC₃T_r MXene, the polarization charge generation process under the external stress is illustrated in Fig. 3. The TiVCrMoC₃T_r monolayer exhibits a hexagonal lattice formed by four metal elements (Ti, V, Cr, and Mo) and C atoms, terminated by surface functional groups (Fig. 3a) [13]. The multi-atomic structure and the asymmetric functional groups could induce the inversion symmetry breaking in the crystal structure [9,40,41]. At the original state, the electric dipole moments (P_1, P_2, P_3) in the metal- T_x hexagonal structure unit cancel each other $(P_1 + P_2 + P_3 = 0, left inset of Fig. 3b)$. Upon strain applied (right inset of Fig. 3b), increased P₁ and reduced P2 and P3 shift the charge centers, thus positive and negative ionic polarization charges would be accumulated accordingly, creating directional piezoelectric field. Similarly, metal-C bond stretching disrupts the equilibrium of dipole moments (P₄, P₅ and P₆), producing secondary polarization, though its contribution to piezoelectricity is minor compared to the dominant metal- T_x bond (Fig. 3c). The primary piezoelectric response arises from the non-centrosymmetric lattice distortion induced by terminal functional groups and the asymmetric multi-atomic structure [5,15]. Given its repeating metal- T_x and metal-C units and the asymmetric metallic atom distribution, the TiVCrMoC₃T_x MXene exhibits piezoelectricity under mechanical deformation. Moreover, while the outer metal layers in TiVCrMoC₃T_x exhibit various segregation tendencies, a distinct asymmetric interlayer atom segregation could be observed

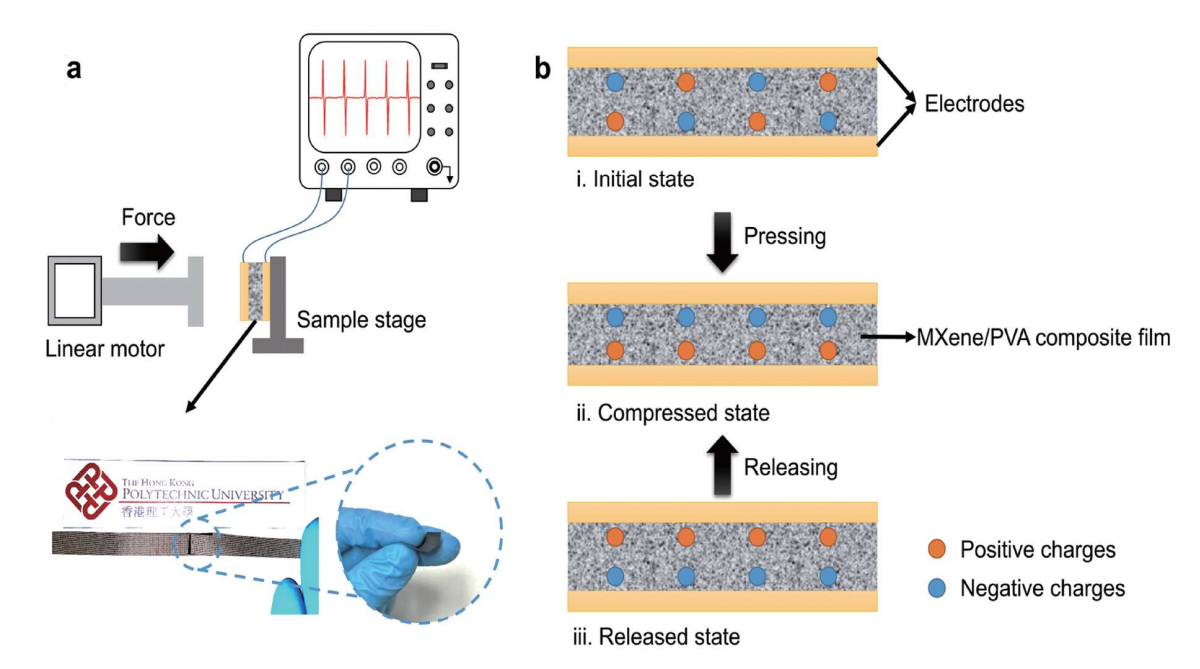


Figure 2 (a) Experimental setup for output performance testing. Inset: the MXene/PVA-PENG device and the MXene-PVA composite film. Inset: flexible MXene-PVA composite film. (b) Schematic illustration for the energy conversion process in MXene/PVA PENG. (i) Initial state, (ii) compressed state and (iii) released state.

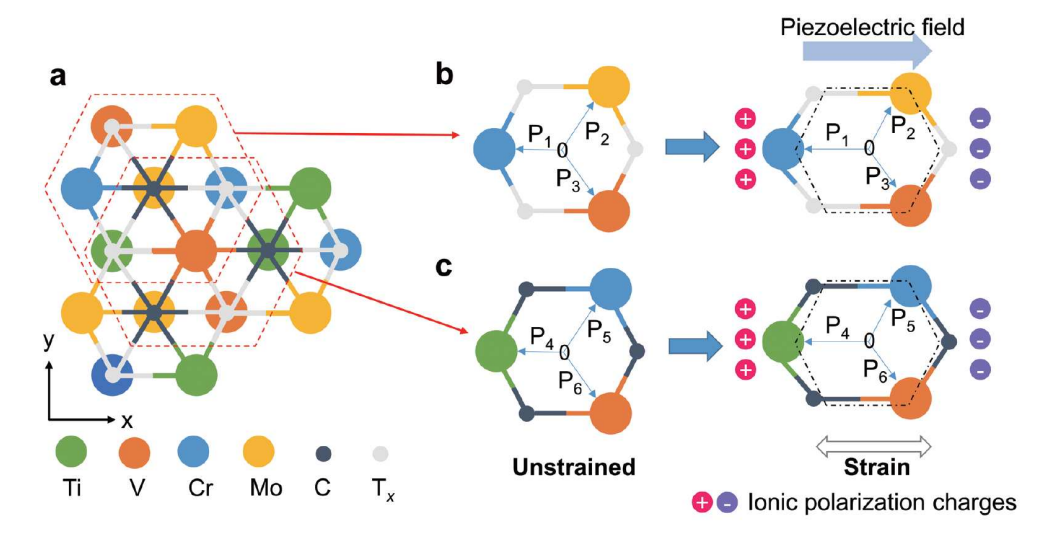


Figure 3 The generation of piezoelectric field in $TiVCrMoC_3T_x$ by an external strain. (a) Top view of $TiVCrMoC_3T_x$ structure. (b) Simplified metal- T_x hexagonal structure. (c) Metal-C hexagonal structure.

within TiVCrMoC₃T_x [15]. This asymmetric behavior may affect the polarization and charge separation processes in TiVCrMoC₃T_x, revealing its ability to generate piezoelectric charges and respond to electric fields or mechanical stimuli.

Fig. 2b illustrates the fundamental principle of converting mechanical energy into electrical energy in the MXene/PVA-PENG. At the initial state (i), the charges in the nanogenerator are maintained at an equilibrium state. As a compressive force is applied to the device (ii), the opposite positive and negative charges in the MXene/PVA-PENG will go towards the electrodes respectively in response to the mechanical stimulus, which is attributed to a polarization effect from the composite film. This charge separation leads to an electric field in the internal circuit, and then it will be transferred as the positive output signals (selfpowered output). Once the force is released (iii), the charges flow back, and the negative output signals can be obtained. Therefore, the mechanical energy could be successfully converted into electrical energy in this MXene/PVA-PENG. The whole process could work without the supply of external electrical fields, which confirms the self-powered capability. Besides, the interfacial polarization at the heterogeneous boundaries between MXene nanosheets and the PVA matrix creates localized electric fields under mechanical stress. These fields facilitate the realignment of dipoles within both the polymer chains and the surface functional groups of MXene, thereby amplifying the strain-induced polarization. The mechanically induced alignment of dipoles in the PVA and at the MXene surfaces, facilitated by interfacial polarization, results in an efficient and coordinated polarization response [20,35]. Although the MXene-PVA composite film does not exhibit ferroelectric characteristics, its notable piezoelectric response can be attributed to interfacial polarization at the MXene/PVA interface, the high-entropy effects, the presence of functional groups on MXene nanosheets, and strain-induced dipole alignment within the polymer matrix. These synergistic effects collectively contribute to the observed piezoelectric behavior in the MXene/ PVA composite [5,42].

The output performance of the MXene/PVA-PENG is demonstrated in Fig. 4. The output voltage and current signals of MXene/PVA-PENG were 500 mV and 790 pA at 3.47 N com-

pressive force, respectively (Fig. 4a, b). It is evident that a positive output piezoresponse is generated under the applied compressive strain. Upon removing the strain from the device, the output voltage and current exhibit corresponding shifts towards negative values. The output signals exhibit an increase with the applied force ranging from 1.96 to 3.47 N (Fig. 4c, d). Compared to previously reported MXene-based PENGs [5,9] (as shown in Supplementary material, Table S2), the MXene/PVA-PENG delivers a significantly higher output voltage while maintaining a comparable output current. Although the power density appears lower due to the relatively larger device size, the high voltage output demonstrates the enhanced piezoelectric response of our device. These results highlight the great potential of the MXene/PVA-PENG for future applications in high-sensitivity self-powered sensors and mechanical energy harvesting. Moreover, the peak output current remains stable over 1500 cycles at 1.96 N force (Fig. 4e, f), affirming the good mechanical durability of the high-quality MXene/PVA-PENG, enabling their practical use in wearable electronics and self-powered sensors. The voltage and current under different load resistances were also measured to observe how the PENG responds to varying external loads, as shown in Fig. 5a-c. The voltage increased with the increasing load resistors, while the current signals were opposite. The output power obtained from multiplying the voltage and current could reach up to 110.76 pW, allowing for practical applications for low-power systems. The polarity of the output signal was found to reverse with the direction of applied strain, consistent with the characteristics of piezoelectricity rather than triboelectricity (Supplementary material, Fig. S7). Additionally, control experiments using pristine PVA further verified that the output signal originated from the MXene-PVA composite itself (Supplementary material, Fig. S8). These results collectively confirm that the measured signals are predominantly due to the piezoelectric response of the MXene/PVA composite film, rather than triboelectric artifacts.

We also compare diverse approaches to flexible energy harvesting, with MXene-based materials emerging as particularly promising for nanogenerators. This MXene-PVA composite film performed well by addressing key limitations: its high-entropy $TiVCrMoC_3T_x$ MXene, synthesized via feasible HF-free etching,

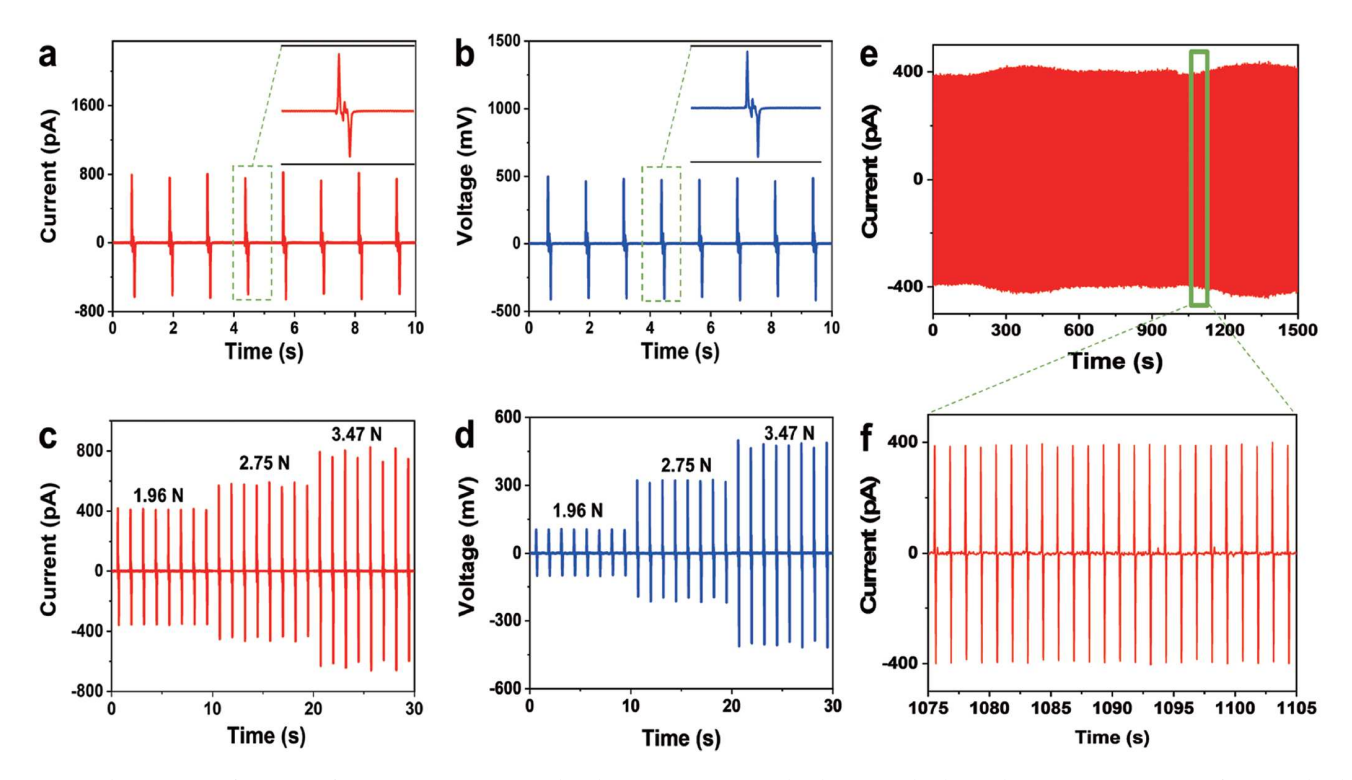


Figure 4 The output performance of MXene/PVA-PENG. (a, b) The output current and voltage signals obtained at 3.47 N compressive force. (c, d) The output signals obtained at different forces. (e, f) Cyclic durability test for 1500 cycles at 1.96 N and its corresponding enlarged image from the green box.

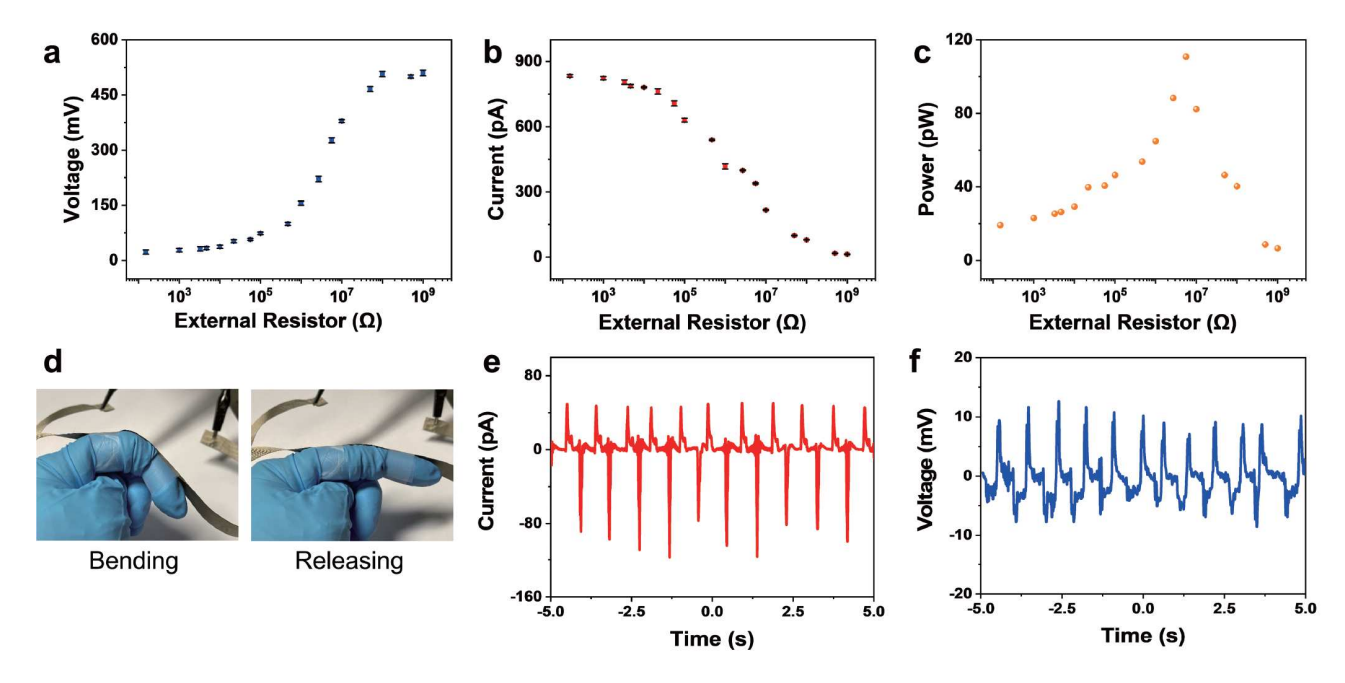


Figure 5 Output performance of MXene/PVA-PENG under different external load resistance and output signals of self-powered sensor based on MXene-PVA composite film. (a) Open-circuit voltages. (b) Short-circuit currents. (c) Output powers. (d) Finger motion monitoring while bending and releasing. (e, f) The corresponding output current and voltage signals obtained from finger motion.

exhibits a robust piezoelectric response (500 mV, 790 pA at 3.47 N) due to asymmetric lattice structure and hydrogen bonding with PVA, which enhances mechanical flexibility (1500-cycle durability) and biocompatibility. Unlike thermoelectric, it operates independently of temperature gradients [43]; compared to TENGs, it avoids crosstalk and humidity issues [44]; and relative to P(VDF-TrFE) (PVDF)-based systems, it

delivers higher output signals [45,46]. The synergy of high piezoresponse, environmental resilience, and biocompatibility in MXene-PVA composite film positions it as a good candidate for wearable and biomedical PENGs. On these bases, the flexible nanogenerators based on high-entropy MXene-PVA composite demonstrated their potential in energy harvesting and nanodevice powering.

Based on the well-performed piezoelectric outputs, the flexible MXene/PVA-PENG was further integrated onto the finger to function as a self-powered motion monitoring sensor. Upon bending and releasing the finger, distinct positive and negative output signals were generated and collected (Fig. 5d). Notably, these signals were recorded in the absence of any external bias, confirming the device's self-powered operation. The measured current and voltage output (Fig. 5e, f) reached approximately 85 pA and 10 mV, respectively, indicating good sensitivity and robust performance of the MXene/PVA-PENG sensor. These findings highlight the considerable potential of the MXene/PVA-PENG device for applications in wearable electronics.

CONCLUSIONS

In summary, we have demonstrated MXene-PVA composite films with high stability and mechanical strength for high-performance flexible piezoelectric nanogenerators. The high-entropy piezoelectric TiVCrMoC $_3$ T $_x$ MXene layered nanosheets synthesized via the thermal-assisted electrochemical etching method exhibit highly crystalline structure. Furthermore, the formation of strong hydrogen bonding between MXene nanosheets and PVA facilitates good flexibility, stability and biocompatibility. These combined advantages contribute to high-performance self-powered energy harvesting in MXene/PVA-PENG, exhibiting good durability and achieving high output power of up to 110.76 pW. The MXene-PVA composite films exhibit good mechanical stability and high piezoelectric response, revealing significant promise for application in self-powered electronics and wearable technologies.

Received 24 February 2025; accepted 28 May 2025; published online 3 July 2025

- 1 Zhang J, Zhao Y, Guo X, et al. Single platinum atoms immobilized on an MXene as an efficient catalyst for the hydrogen evolution reaction. Nat Catal, 2018, 1: 985–992
- 2 Zha XH, Yin J, Zhou Y, et al. Intrinsic structural, electrical, thermal, and mechanical properties of the promising conductor Mo₂C MXene. J Phys Chem C, 2016, 120: 15082–15088
- 3 Lipatov A, Lu H, Alhabeb M, et al. Elastic properties of 2D Ti₃C₂T_x MXene monolayers and bilayers. Sci Adv, 2018, 4: eaat0491
- 4 Wyatt BC, Rosenkranz A, Anasori B. 2D MXenes: tunable mechanical and tribological properties. Adv Mater, 2021, 33: e2007973
- 5 Tan D, Jiang C, Sun N, et al. Piezoelectricity in monolayer MXene for nanogenerators and piezotronics. Nano Energy, 2021, 90: 106528
- 6 Wang D, Zhang D, Li P, et al. Electrospinning of flexible poly(vinyl alcohol)/MXene nanofiber-based humidity sensor self-powered by monolayer molybdenum diselenide piezoelectric nanogenerator. Nano-Micro Lett, 2021, 13: 57
- 7 Jin L, Ao Y, Xu T, et al. Recent advances in MXene-based composites for piezoelectric sensors. Nanoscale, 2024, 16: 21673–21696
- 8 Pang SY, Wong YT, Yuan S, et al. Universal strategy for HF-free facile and rapid synthesis of two-dimensional MXenes as multifunctional energy materials. J Am Chem Soc, 2019, 141: 9610–9616
- 9 Jiang C, Zeng L, Tan D, et al. Piezoelectric behavior of single-layer oxidized-MXene for nanogenerators and piezotronics. Nano Energy, 2023, 114: 108670
- 10 Kim G, Yun J, Kim D. Enhancing power generation with a SnSe₂-MXene composite in a piezo-triboelectric hybrid nanogenerator for autonomous energy applications. Nano Energy, 2024, 126: 109678
- 11 Tan J, Wang Y, Wang Z, et al. Large out-of-plane piezoelectricity of oxygen functionalized MXenes for ultrathin piezoelectric cantilevers and diaphragms. Nano Energy, 2019, 65: 104058
- 12 Pang SY, Io WF, Guo F, et al. Two-dimensional MXene-based devices

- for information technology. Mater Sci Eng-R-Rep, 2025, 163: 100894
- 13 Nemani SK, Zhang B, Wyatt BC, et al. High-entropy 2D carbide MXenes: TiVNbMoC₃ and TiVCrMoC₃. ACS Nano, 2021, 15: 12815– 12825
- 14 Tan TL, Jin HM, Sullivan MB, et al. High-throughput survey of ordering configurations in MXene alloys across compositions and temperatures. ACS Nano, 2017, 11: 4407–4418
- 15 Leong Z, Jin H, Wong ZM, et al. Elucidating the chemical order and disorder in high-entropy MXenes: a high-throughput survey of the atomic configurations in TiVNbMoC₃ and TiVCrMoC₃. Chem Mater, 2022, 34: 9062–9071
- 16 Li Y, Shao H, Lin Z, et al. A general Lewis acidic etching route for preparing MXenes with enhanced electrochemical performance in nonaqueous electrolyte. Nat Mater, 2020, 19: 894–899
- 17 Li T, Yao L, Liu Q, et al. Fluorine-free synthesis of high-purity ${\rm Ti_3C_2T_x}$ (T = OH, O) via alkali treatment. Angew Chem Int Ed, 2018, 57: 6115–6119
- 18 Ma R, Zhang X, Zhuo J, et al. Self-supporting, binder-free, and flexible Ti₃C₂T_x MXene-based supercapacitor electrode with improved electrochemical performance. ACS Nano, 2022, 16: 9713–9727
- 19 Ling Z, Ren CE, Zhao MQ, et al. Flexible and conductive MXene films and nanocomposites with high capacitance. Proc Natl Acad Sci USA, 2014, 111: 16676–16681
- 20 Zhao L, Wang L, Zheng Y, et al. Highly-stable polymer-crosslinked 2D MXene-based flexible biocompatible electronic skins for in vivo biomonitoring. Nano Energy, 2021, 84: 105921
- 21 Naguib M, Kurtoglu M, Presser V, et al. Two-dimensional nanocrystals produced by exfoliation of Ti₃AlC₂. Adv Mater, 2011, 23: 4248–4253
- 22 Cheng L, Chen Q, Li J, et al. Boosting the photocatalytic activity of CdLa₂S₄ for hydrogen production using Ti₃C₂ MXene as a co-catalyst. Appl Catal B-Environ, 2020, 267: 118379
- 23 Cao S, Shen B, Tong T, et al. 2D/2D heterojunction of ultrathin MXene/ Bi₂WO₆ nanosheets for improved photocatalytic CO₂ reduction. Adv Funct Mater, 2018, 28: 1800136
- 24 Spanier JE, Gupta S, Amer M, *et al.* Vibrational behavior of the $M_{n+1}AX_n$ phases from first-order Raman scattering (M = Ti, V, Cr, A = Si, X = C, N). Phys Rev B, 2005, 71: 012103
- Lai S, Jeon J, Jang SK, et al. Surface group modification and carrier transport properties of layered transition metal carbides (Ti₂CT_x, T: –OH, –F and –O). Nanoscale, 2015, 7: 19390–19396
- 26 Dixit P, Maiti T. A facile pot synthesis of (Ti₃AlC₂) MAX phase and its derived MXene (Ti₃C₂T_x). Ceramics Int, 2022, 48: 36156–36165
- 27 Liu F, Zhou A, Chen J, et al. Preparation and methane adsorption of two-dimensional carbide Ti₂C. Adsorption, 2016, 22: 915–922
- 28 Ferrari AC, Robertson J, Ferrari AC, et al. Raman spectroscopy of amorphous, nanostructured, diamond-like carbon, and nanodiamond. Philos Trans R Soc London Ser A-Math Phys Eng Sci, 2004, 362: 2477– 2512
- 29 Kumar S. Fluorine-free MXenes: recent advances, synthesis strategies, and mechanisms. Small, 2024, 20: 2308225
- 30 Yoon J, Kim S, Park KH, *et al.* Biocompatible and oxidation-resistant $Ti_3C_2T_x$ MXene with halogen-free surface terminations. Small Methods, 2023, 7: 2201579
- 31 Yang F, Li J, Long Y, et al. Wafer-scale heterostructured piezoelectric bio-organic thin films. Science, 2021, 373: 337–342
- 32 Liu J, Zhang H, Sun R, *et al.* Hydrophobic, flexible, and lightweight MXene foams for high-performance electromagnetic-interference shielding. Adv Mater, 2017, 29: 1702367
- 33 Xie Y, Jiang W, Fu T, et al. Achieving high energy density and low loss in PVDF/BST nanodielectrics with enhanced structural homogeneity. ACS Appl Mater Interfaces, 2018, 10: 29038–29047
- 34 Wan YJ, Li XM, Zhu PL, et al. Lightweight, flexible MXene/polymer film with simultaneously excellent mechanical property and high-performance electromagnetic interference shielding. Compos Part A-Appl Sci Manufacturing, 2020, 130: 105764
- 35 Mirkhani SA, Shayesteh Zeraati A, Aliabadian E, et al. High dielectric constant and low dielectric loss via poly(vinyl alcohol)/Ti₃C₂T_x MXene nanocomposites. ACS Appl Mater Interfaces, 2019, 11: 18599–18608
- 36 Shepelin NA, Sherrell PC, Skountzos EN, et al. Interfacial piezoelectric

SCIENCE CHINA Materials

ARTICLES

polarization locking in printable $Ti_3C_2T_x$ MXene-fluoropolymer composites. Nat Commun, 2021, 12: 3171

- 37 Yang B, Liu Y, Lan S, et al. High-entropy design for dielectric materials: Status, challenges, and beyond. J Appl Phys, 2023, 133: 110904
- 38 Wu J, Ma X, Zhou D, et al. High-entropy high-temperature high-pie-zoelectricity ceramics. Adv Mater, 2025, 37: 2419134
- 39 Chen Y, Tian Z, Wang X, et al. 2D transition metal dichalcogenide with increased entropy for piezoelectric electronics. Adv Mater, 2022, 34: 2201630
- 40 Tan D, Sun N, Chen L, et al. Piezoelectricity in monolayer and multilayer Ti₃C₂T_x MXenes: implications for piezoelectric devices. ACS Appl Nano Mater, 2022, 5: 1034–1046
- 41 Li X, Qiu J, Cui H, et al. Machine learning accelerated discovery of functional MXenes with giant piezoelectric coefficients. ACS Appl Mater Interfaces, 2024, 16: 12731–12743
- 42 Deng Q, Zhou F, Qin B, et al. Eco-friendly poly(vinyl alcohol)/delaminated V₂C MXene high-k nanocomposites with low dielectric loss enabled by moderate polarization and charge density at the interface. Ceramics Int, 2020, 46: 27326–27335
- 43 Li J, Xia B, Xiao X, et al. Stretchable thermoelectric fibers with threedimensional interconnected porous network for low-grade body heat energy harvesting. ACS Nano, 2023, 17: 19232–19241
- 44 Li J, Liu Y, Wu M, et al. Thin, soft, 3D printing enabled crosstalk minimized triboelectric nanogenerator arrays for tactile sensing. Fundamental Res, 2023, 3: 111–117
- 45 Hu Q, Wan X, Wang S, et al. Ultrathin, flexible, and piezoelectric Janus nanofibrous dressing for wound healing. Sci China Mater, 2023, 66: 3347–3360
- 46 Dai B, Gao C, Guo J, et al. A robust pyro-phototronic route to markedly enhanced photocatalytic disinfection. Nano Lett, 2024, acs.nanolett.3c05098

Acknowledgement This work was supported by the Research Grants Council of Hong Kong (GRF no. 15303123), Research Grants Council of Hong Kong (PolyU SRFS 2122-5S02), and PolyU Projects of the Research Centre for Nanoscience and Nanotechnology (RCNN) and the Photonics Research Institute (PRI) (1-CE0H and 1-CD6X).

Funding note Open Access funding provided by The Hong Kong Polytechnic University.

Author contributions Yang F, Pang S-Y and Hao J conceived the idea, designed the experiments, and engineered the samples; Yang F, Chan K L, and Zhao F performed the experiments; Yang F, Wu Z, Wong M C and Pang S-Y performed the data analysis; Yang F wrote the paper with support from Hao J. All authors contributed to the general discussion.

Conflict of interest The authors declare that they have no conflict of interest.

Supplementary information Supplementary materials are available in the online version of the paper.

Open Access This article is licensed under a Creative Commons Attribution 4.0 International License, which permits use, sharing, adaptation, distribution and reproduction in any medium or format, as long as you give appropriate credit to the original author(s) and the source, provide a link to the Creative Commons licence, and indicate if changes were made.

The images or other third party material in this article are included in the article's Creative Commons licence, unless indicated otherwise in a credit line to the material. If material is not included in the article's Creative Commons licence and your intended use is not permitted by statutory regulation or exceeds the permitted use, you will need to obtain permission directly from the copyright holder.

To view a copy of this licence, visit http://creativecommons.org/licenses/by/4.0/.



Fumei Yang received her MS degree from Shenzhen University in 2020. She is currently a PhD candidate under the supervision of Prof. Jianhua Hao in the Department of Applied Physics, The Hong Kong Polytechnic University (PolyU). Her current research focuses on the synthesis of 2D materials and piezoelectric nanogenerators.



Jianhua Hao is a Chair Professor of Materials Physics and Devices and Director of the Research Centre for Nanoscience and Nanotechnology at PolyU. His research interests include metal-ion-doped luminescent materials and devices, functional thin films, and heterostructures.

无氢氟酸合成的高熵MXene-PVA复合薄膜及其柔性 纳米发电机

杨富美, 陳錦煉, 吴泽涵, 赵芳青, 黄文聰, 彭倩兒, 郝建华*

摘要 MXene表现出显著的压电性能,使其成为下一代智能可穿戴设备和生物电子学中高性能压电纳米发电机(PENGs)应用的潜力材料。然而,当前基于MXene的压电纳米发电机面临诸多挑战,例如机械强度不足、压电响应较低以及长期工作稳定性有限。这些问题主要源于MXene纳米片的有效应力传递面积较小以及应变水平较低。在本研究中,我们通过利用MXene与聚乙烯醇(PVA)之间的强氢键相互作用,构建了一种高熵TiVCrMoC₃T_x MXene复合薄膜,并进一步开发出一种自供电柔性纳米发电机。该器件在受到3.47 N的压力时输出高达500 mV和790 pA的压电信号,且在1500个循环工作过程中表现出良好的长期工作稳定性。此外,该高熵MXene纳米片通过无氢氟酸(HF-free)蚀刻方法合成,确保了其在生物电子学应用中的安全性和生物相容性。本工作突显了高熵MXene在柔性可穿戴电子产品和能量收集方面的可持续应用潜力。